THE UNIVERSITY of EDINBURGH

Edinburgh Research Explorer

Targeted design leads to tunable photoluminescence from perylene dicarboxdiimide-poly(oxyalkylene)/siloxane hybrids for luminescent solar concentrators

Citation for published version:
Meazzini, I, Willis-Fox, N, Blayo, C, Arlt, J, Clement, S & Evans, RC 2016, 'Targeted design leads to tunable photoluminescence from perylene dicarboxdiimide-poly(oxyalkylene)/siloxane hybrids for luminescent solar concentrators', *Journal of Materials Chemistry C Materials for optical and electronic devices*, vol. 4, no. 18, pp. 4049-4059. https://doi.org/10.1039/C5TC03952E

Digital Object Identifier (DOI):
10.1039/C5TC03952E

Link:
Link to publication record in Edinburgh Research Explorer

Document Version:
Publisher's PDF, also known as Version of record

Published In:
Journal of Materials Chemistry C Materials for optical and electronic devices

General rights
Copyright for the publications made accessible via the Edinburgh Research Explorer is retained by the author(s) and / or other copyright owners and it is a condition of accessing these publications that users recognise and abide by the legal requirements associated with these rights.

Take down policy
The University of Edinburgh has made every reasonable effort to ensure that Edinburgh Research Explorer content complies with UK legislation. If you believe that the public display of this file breaches copyright please contact openaccess@ed.ac.uk providing details, and we will remove access to the work immediately and investigate your claim.

OPEN ACCESS

Download date: 12. Oct. 2024

Journal of
Materials Chemistry C

PAPER

Cite this: J. Mater. Chem. C, 2016, 4, 4049

Targeted design leads to tunable photoluminescence from perylene dicarboxdiimide–poly(oxyalkylene)/siloxane hybrids for luminescent solar concentrators†

Ilaria Meazzini,[a] Niamh Willis-Fox,[a] Camille Blayo,[a] Jochen Arlt,[b] Sébastien Clément[c] and Rachel C. Evans*[a]

Received 24th November 2015,
Accepted 23rd March 2016

DOI: 10.1039/c5tc03952e

www.rsc.org/MaterialsC

A series of organic–inorganic hybrid materials in which a perylene carboxdiimide-bridged triethoxysilane (**PDI-Sil**) is covalently grafted to the siliceous domains of poly(oxyalkylene)/siloxane hybrids from the ureasil family has been synthesised (**PDI-Sil**-ureasils), with the aim of tailoring the optical properties towards their future application in luminescent solar concentrators (LSCs). Steady-state and time-resolved photoluminescence studies revealed that the ureasil host is able to isolate **PDI-Sil**, which inhibits the formation of aggregates. The ureasil also functions as an active host, with its intrinsic photoluminescence contributing to the optical properties of the hybrid material. Through strategic variation of the branching and molecular weight of the poly(oxyalkylene) backbone, it was shown that the efficiency of energy transfer from the ureasil host to the **PDI-Sil** can be modulated, which tunes the emission colour from pink to orange. The chain length, rather than the number of branches, on the poly(oxyalkylene) backbone was shown to influence the photoluminescence most significantly. Since ureasils demonstrate waveguiding properties, the results indicate that covalent grafting of a fluorophore directly to a waveguide host may provide an attractive route to more efficient LSCs.

Introduction

Organic semiconductors, such as π-conjugated polymers and π-conjugated molecular systems, underpin the development of most emerging flexible optoelectronic technologies, including light-emitting displays, organic photovoltaic devices, field effect transistors and optical sensors.[1–6] The performance of such devices depends critically on both the electronic and optical properties of the active molecule and its molecular packing or morphology in the solid-state.[7,8] For the design of light-emitting materials, in particular, transfer of a fluorophore from solution to the solid-state frequently leads to significant quenching of photoluminescence due to the aggregation of discrete molecules and/or the re-absorption of emitted light.[9,10] The incorporation of the fluorophore into a host can inhibit intermolecular interactions and the resultant quenching, while simultaneously enhancing the mechanical and optical stability at the macroscale.[11,12] However, such systems are often susceptible to intrinsic phase separation due to the physicochemical dissimilarity of the two components.[13] This is particularly challenging for glassy matrices prepared *via* the sol–gel process, due to poor miscibility between the hydrophilic inorganic oxide precursors and the hydrophobic π-conjugated polymer or molecule.[14] For host–guest systems, where the lumophore is physically trapped in the matrix (so-called Class I hybrids), cooperative interactions (*e.g.* hydrogen bonding, ionic, van der Waals, π–π stacking) at the interface play a crucial role in determining phase miscibility[15–17] and the orientation of individual components.[18–20] However, with suitable chemical functionalisation of the π-conjugated molecule, for example through the addition of reactive alkoxysilane groups, they can be covalently-grafted to a silica framework, forming a Class II organic–inorganic hybrid.[21–25] This offers the advantage of increased lumophore loading and improved stability of the resultant material.

For extended π-conjugated molecules, however, covalent grafting may still not enable sufficient miscibility with a purely inorganic oxide matrix. In this context, a host material which is

[a] School of Chemistry and CRANN, Trinity College, The University of Dublin, Dublin 2, Ireland. E-mail: raevans@tcd.ie
[b] Collaborative Optical Spectroscopy, Micromanipulation and Imaging Centre (COSMIC) and SUPA, School of Physics and Astronomy, University of Edinburgh, King's Buildings, EH9 3JZ, UK
[c] Institut Charles Gerhardt – UMR 5253, Université de Montpellier – CC1701, Place Eugène Bataillon, F-34095 Montpellier Cedex 05, France

† Electronic supplementary information (ESI) available: Materials, synthesis and characterisation of **PDI-Sil**, structural characterisation (powder XRD diffractograms, ^{29}Si and ^{13}C CP MAS-NMR spectra, FTIR fitting data), stability studies (TGA and photodegradation), UV/Vis absorption spectra, supplementary steady-state photoluminescence data, ps-emission decay lifetime fitting data and procedure, supplementary fluorescence anisotropy data. See DOI: 10.1039/c5tc03952e

This journal is © The Royal Society of Chemistry 2016

itself an organic–inorganic hybrid material may be preferable. The ureasils, a family of Class II hybrids, have attracted considerable attention as functional hosts for diverse optical applications including solid-state electrochromic devices,[26] components of full-colour displays[27,28] and as optical waveguides.[29,30] Ureasils are comprised of a siliceous skeleton that is chemically-grafted to poly(oxyalkylene) chains *via* urea [NHC(═O)HN] bridges. They are intrinsically photoluminescent and have been frequently used as an active host for non-grafted lanthanide ions/complexes,[31,32] molecular dyes[33] and more recently π-conjugated polymers,[28,34] in which the excitation wavelength dependence of the ureasil emission is used to tune the extent of energy transfer between the host and the dopant. Ureasils can be processed as transparent free-standing monoliths or as thin films or coatings, and exhibit relatively high refractive indices (∼1.49).[29] The latter property has led to their recent consideration as waveguide slabs/films for luminescent solar concentrators (LSCs).[32,33]

In this paper, we report the strategic design of ureasil-type hybrid materials which contain a π-conjugated perylene carboxdiimide-bridged triethoxysilane (**PDI-Sil**), covalently grafted to the siliceous framework. Perylene carboxdiimides are frequently employed as archetypal lumophores in LSCs due to their high molar absorption coefficients, excellent photoluminescence quantum yields and good photostability.[35] However, the optical efficiency of LSCs incorporating perylene diimides purely through doping is often low due to lumophore aggregation and/or reabsorption losses.[36] Donor–acceptor energy transfer cascades have recently been shown to effectively minimise reabsorption losses in LSCs.[37,38] Here, we adopt a different approach and attempt to spatially isolate the lumophore within the waveguide host, inhibiting aggregation. To achieve this we exploit the commercial availability of polyether amines (Jeffamine®)[39] presenting linear (diamine) and tripodal (triamine) branching and different chain lengths, in an attempt to control the placement of **PDI-Sil** within the resultant ureasil monolith. Given that the packing and orientation of individual molecules mediates their electronic coupling, we postulated that this approach may provide a route to reducing reabsorption events and/or aggregation of the lumophore within the host matrix, thereby leading to higher optical efficiencies.

Experimental

Instrumentation and methods

All reactions were carried out under argon using standard high-vacuum and Schlenk techniques. ^{1}H, ^{13}C{^{1}H} were recorded with a Bruker Avance 600 spectrometer (^{1}H 600.26 MHz, ^{13}C{^{1}H} 150.96 MHz). ^{29}Si{^{1}H} was acquired on a Bruker Avance 400 spectrometer (79.46 MHz). All chemical shifts and coupling constants are reported in ppm and Hz, respectively.

Fourier transform infrared (FTIR) spectra were recorded on a Perkin-Elmer spectrum 100 FTIR spectrometer at room temperature. FTIR spectra were collected over a range of 4000–400 cm^{-1} by averaging 64 scans at a resolution of 4 cm^{-1}. The samples (2 mg) were finely ground and mixed with potassium bromide (175 mg) and pressed into pellets. To evaluate the contributions to the Amide I band spectral deconvolution using Gaussian band fitting was carried out using Origin 8.0® (Microcal) in the region of 1600–1800 cm^{-1}. Mass spectrometry (MS) analysis was performed with a Q-ToF Premier Waters MALDI-quadrupole time-of-flight (ToF) spectrometer equipped with a matrix-assisted laser desorption–ionisation (MALDI) source, using Glu-1-Fibrinopetide B as the MALDI matrix (reference peak of m/z = 1570.6774). Electrospray ionisation (ESI) mass spectrometry was performed on an ESI-TOF Q instrument in positive mode.

Powder X-ray diffraction (PXRD) patterns were recorded using a Bruker D2 Phaser diffractometer. The samples were exposed to Cu K$_{\alpha}$ radiation (λ = 1.54 Å) at room temperature in the range 5–70° (2θ). Solid-state ^{29}Si and ^{13}C cross-polarised (CP) and directly-excited (DE) nuclear magnetic resonance (NMR) spectroscopy were performed at ambient temperature on a Varian VNMRS instrument operating at 79.44 MHz for ^{29}Si and 100.56 MHz for ^{13}C. Spectra were recorded against an external tetramethyl silane (TMS) standard with magic angle spinning (MAS) at a spinning rate of 6000–10 000 Hz. The ^{13}C CP spectra were obtained as single contact experiments with a contact time of 1 ms and a recycle delay of 5.0 s (repetitions varying between 168 and 600). Thermogravimetric analysis was performed using a Perkin Elmer Pyris 1 TGA thermogravimetric analyser in the range 30–900 °C in an air atmosphere using *ca.* 2 mg sample, at a heating rate of 10 °C min^{-1} in a ceramic crucible. The instrument was calibrated against In and Ni standards in an air atmosphere.

UV/Vis absorption spectra were recorded using a Perkin Elmer Lambda 1050 UV/Vis scanning spectrometer. Steady-state photoluminescence (PL) spectroscopy was performed on a Fluorolog-3 spectrophotometer (Horiba Jobin Yvon), using the front-face configuration for solid-state samples. The emission and excitation slit widths were fixed at 1 nm. Photoluminescence quantum yields were measured using a F-3018 integrating sphere accessory mounted on a FluoroMax-4 spectrophotometer (Horiba Jobin Yvon). The values reported are the mean of three repeat measurements. The method is accurate to within 10%. Emission and excitation spectra were corrected for the wavelength response of the system and the intensity of the lamp profile over the excitation range, respectively, using correction factors supplied by the manufacturer. Steady-state fluorescence anisotropy experiments were carried out using a Jobin-Yvon Fluorolog-3 spectrometer with right angle geometry and excitation and emission slits of 2 and 1 nm, respectively.

Fluorescence decays were measured using the picosecond time-correlated single photon counting (TCSPC) method at the Collaborative Optical Spectroscopy, Micromanipulation and Imaging Centre (COSMIC), University of Edinburgh, UK. The excitation source was the second harmonic of the pulse-picked output of a Ti-Sapphire femtosecond laser system (Coherent, 10 W Verdi and Mira Ti-Sapphire), delivering pulses of ∼200 fs at 4.75 MHz repetition rate. Fluorescence decays were measured using an Edinburgh Instruments spectrometer equipped with TCC900 photon counting electronics. The instrument response of the system was ∼90 ps full-width-half-maximum (FWHM). The decay curves were analysed using a standard iterative

 This journal is © The Royal Society of Chemistry 2016

reconvolution method, assuming a multiexponential decay function. Reconvolution and fitting of the fluorescence decays were carried out using Globals WE® software package as described in the ESI.†[40] The quality of fit was judged on the basis of the reduced chi-square statistic, χ^2, and the randomness of residuals.

Synthesis of *N*,*N*-bis(3-triethoxysilylpropyl)-1,6,7,12-tetra-*tert*-butylphenoxyperylene-3,4:9,10-tetra-carboxdiimide (PDI-Sil)

1,6,7,12-Tetra-*tert*-butylphenoxyperylene-3,4,9,10-tetracarboxylic dianhydride was synthesised following previously reported procedures.[41–43] Into a Schlenk flask containing 1,6,7,12-tetra-*tert*-butylphenoxyperylene-3,4,9,10-tetracarboxylic dianhydride (503 mg, 0.51 mmol) in dry ethanol (150 mL), 3-aminopropyltriethoxysilane (1.45 mL, 6.12 mmol, 12 eq.) was added dropwise. The mixture was then reacted under reflux for two days. After cooling at room temperature, the precipitate was collected by filtration and thoroughly washed with cold ethanol to remove the excess of 3-aminopropyltriethoxysilane. The dark red **PDI-Sil** was obtained in 76% yield. ^{1}H NMR: δ = 0.69–0.72 (m, 4 H, Si–CH$_2$), 1.20 (t, 18H, $^3J_{H-H}$ = 6.8 Hz, OCH$_2$–C*H$_3$*), 1.31 (s, 36 H, C(CH$_3$)$_3$), 1.78–1.83 (m, 4H), 3.79 (q, 12H, $^3J_{H-H}$ = 7.0 Hz, OC*H$_2$*–CH$_3$), 4.12 (t, 4H, $^3J_{H-H}$ = 7.3 Hz, CH$_2$–N), 6.84 (d, 8H, $^3J_{H-H}$ = 8.5 Hz), 7.24 (d, 8H, $^3J_{H-H}$ = 8.8 Hz), 8.23 (s, 4H) ppm. ^{13}C{^{1}H} NMR: δ = 8.2 (Si–CH$_2$); 18.4 (OCH$_2$*C*H$_3$), 21.7 (Si–CH$_2$–*C*H$_2$), 31.6, 34.5, 43.2 (N–*C*H$_2$), 58.5 (OCH$_2$), 119.5, 119.6, 120.1, 120.7, 122.7, 126.8, 133.0, 143.0, 147.4, 153.1, 156.1, 163.5 (C=O) ppm. ^{29}Si{^{1}H} NMR: δ = −46.0 ppm. ESI MS (*m*/*z*) calcd: for $C_{82}H_{99}N_2O_{14}Si_2$, 1391.7 found: 1391.7 (M + H). Anal. calcd for $C_{82}H_{99}N_2O_{14}Si_2$: C 70.76; H 7.10; N 2.01. Found: C 70.53; H 6.96, N 1.88.

Synthesis of ureasils and PDI-Sil-ureasils

Undoped ureasils were synthesised following the general procedure previously reported (Fig. 1).[44,45] The final materials are designated as d-U(X) for the di-ureasils and t-U(X) for the tri-ureasils, where X corresponds to the name of the starting Jeffamine® polyetheramine. Two diamines, Jeffamine ED-600 (M_w = 600 g mol^{-1}, ~4 OCH$_2$CHCH$_3$ repeat units, r.u.) and Jeffamine D-4000 (M_w = 4000 g mol^{-1}, 68 OCH$_2$CHCH$_3$ r.u.), were used to prepare the di-ureasils. Similarly, two triamines, Jeffamine T-403 (M_w = 440 g mol^{-1}, 5–6 OCH$_2$CHCH$_3$ r.u.) and Jeffamine T-5000 (M_w = 5000 g mol^{-1}, 85 OCH$_2$CHCH$_3$ r.u.) were used to prepare the tri-ureasils.

As a representative example, Jeffamine T-403 (0.792 mL, 1.76 mmol) was dissolved in THF (5 mL), to which ICPTES (1.307 mL, 5.28 mmol) was added under stirring, corresponding to 1 : 3 stoichiometric equivalents. The solution was refluxed at 70 °C for 24 h, allowed to cool to room temperature, before the sequential addition of EtOH (0.614 mL), HCl (0.5 M, 0.060 mL) and water (0.142 mL) under stirring to trigger sol formation. The molar ratio of ICPTES : EtOH : HCl : H$_2$O was 176 : 350 : 1 : 265. The resultant solution was cast in a polypropylene mould and covered with Parafilm M®. The sol was allowed to age for 48 h, after which the film was pierced to encourage slow evaporation

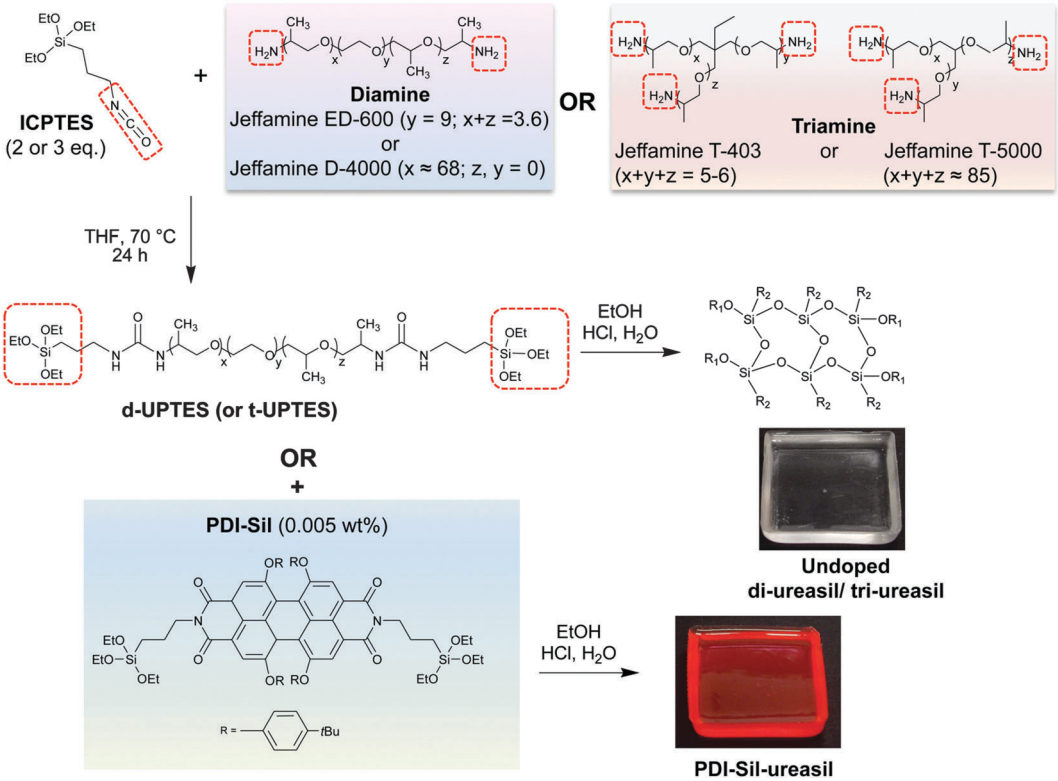

Fig. 1 Targeted synthesis of undoped and **PDI-Sil**-ureasils (R_1 = Si–O–Si– or H, R_2 = –(CH$_2$)$_3$–NHCONH–Jeffamine).

of the solvent from the sample for a further 24 h. The sample was subsequently dried in an oven at 40 °C for 48 h, yielding the resultant **t-U(403)** tri-ureasil as a free-standing, transparent monolith. Synthesis of the analogous **t-U(5000)** tri-ureasil was achieved using the same procedure through substitution with the corresponding Jeffamine T-5000 (1.76 mmol of Jeffamine T-5000 and 5.28 mmol of ICPTES). A larger solvent volume (10 mL) was required to dilute the more viscous, higher MW Jeffamine T-5000. For the di-ureasils, **d-U(600)** and **d-U(4000)**, the ICPTES : Jeffamine ratio was reduced to 2 : 1 to reflect the lower number of primary amine groups in the Jeffamine precursor (3.52 : 1.76 mmol of ICPTES : Jeffamine). Again, a larger sample volume (10 mL) was required to dilute the more viscous D-4000 and the acid concentration was doubled to accelerate gelation (ICPTES : EtOH : HCl : H_2O ratio was 88 : 175 : 1 : 132.5). In addition, an ageing period of 5 days was used for this sample.

A similar approach was employed for the synthesis of **PDI-Sil**-ureasils, with the addition of a stock solution of **PDI-Sil** in THF (0.72 mmol dm^{-3}) under stirring prior to addition of the gelation agents. The mass of gelled precursors was chosen to obtain ∼2 g (mass weighed exactly for each sample) of dried monolith, with the volume of dye solution optimised to ensure a concentration of 0.005% (w/w) in the final sample. **PDI-Sil**-ureasil thick films (0.11 to 0.28 mm) were prepared by drop-casting a mixture of the UPTES precursor, **PDI-Sil** stock solution (0.005% w/w) and the gelation agents, in the same molar ratios as those used for the monoliths, onto cleaned glass substrates. The films were aged overnight in an oven at 40 °C.

Results and discussion

Covalent-grafting of PDI-Sil to ureasil matrices

The synthetic strategy to enable covalent-grafting of **PDI-Sil** to the ureasil host is outlined in Fig. 1. Ureasils are typically prepared in a two step reaction. In the first step, ICPTES is reacted with a commercial Jeffamine® to form the intermediate di- or tri-ureapropyltriethoxysilane (d-UPTES or t-UPTES, respectively), depending on the number of terminal amine groups in the polyetheramine. In the second step, acid-catalysed hydrolysis of the ethoxysilane groups and subsequent condensation results in the formation of the siliceous framework, yielding the corresponding di- or tri-ureasil. We postulated that addition of **PDI-Sil** to the UPTES solution prior to initiation of the sol–gel reaction should result in co-hydrolysis/condensation of the ethoxysilane groups leading to covalent grafting of the dye to the ureasil framework. The acidolysis of **PDI-Sil** under these reaction conditions (pH = 2) was visually confirmed by a change in the solution colour from red to pinkish-purple (Fig. 2a). The *in situ* polymerisation of a structurally-related perylenediimide-bridged-triethoxysilane revealed a similar series of colour transitions as the reaction proceeded.[46] The reaction was also followed by MALDI-TOF mass spectrometry. Following addition of the sol–gel catalyst (aq. acid/EtOH) to a solution of **PDI-Sil** in THF, the M^+ molecular peak (*m*/*z* 1391.66) disappears (Fig. S5, ESI†), and a new peak emerges at *m*/*z* 1222.47, with the predicted isotopic

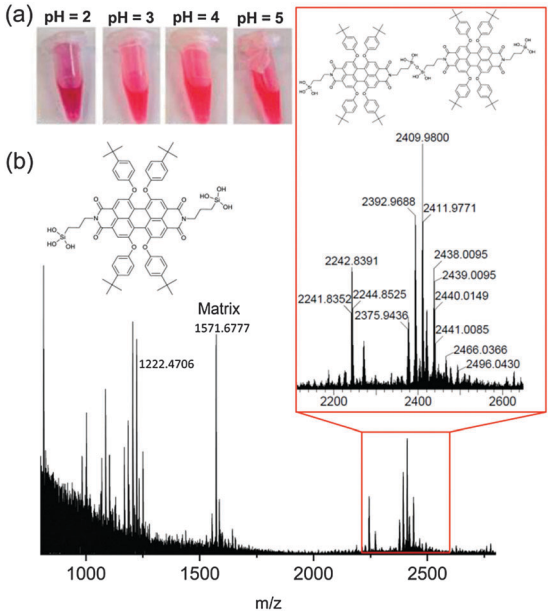

Fig. 2 Acid-catalysed hydrolysis of **PDI-Sil** under the ureasil reaction conditions. (a) Photographs of a **PDI-Sil** solution in THF (10^{-4} mol dm^{-3}) upon ageing at different pH (24 h). (b) MALDI-TOF mass spectrum of the **PDI-Sil** solution following addition of the catalyst (aq. HCl/EtOH).

distribution, assigned to the completely hydrolysed **PDI-Sil**–OH (Fig. 2). In addition, a new population of signals in the high molecular mass region of *m*/*z* 2200–2600 appears, which are assigned to molecular dimers with the loss of hydroxyl groups (*m*/*z* 2409.98 – 1OH, *m*/*z* 2392.01 – 2OH, *m*/*z* 2375.94 – 3OH) and *t*-butylphenyl units (*m*/*z* 2242.84 – 3OH, 1 *t*-butylphenyl). The concentration-dependent formation of stacked dimers has recently been shown to result in a series of chromic shifts in the UV/Vis absorption spectrum of a perylene ammonium derivative.[47] We similarly attribute the gradual change in the solution colour of **PDI-Sil** (pH 2) to the formation of molecular dimers, followed by their subsequent stacking. The stacking process is believed to be concentration-dependent (≥10^{-4} mol dm^{-3}), as no change is observed in the UV/Vis absorption spectrum at lower concentrations (Fig. S6, ESI†). Since **PDI-Sil** is introduced into the ureasil at ∼10^{-5} mol dm^{-3}, stacking effects are not expected to be important.

Four different Jeffamines® were used to investigate the effect of chain length and branching on the orientation of the grafted **PDI-Sil** within the ureasil matrix: Jeffamine ED-600 and D-4000 are both linear macromolecules presenting two amine groups, while Jeffamine T-403 and Jeffamine T-5000 are tri-branched macromolecules with three amine groups. The gelation time was found to be highly dependent on the polyetheramine precursor, taking just 10 min for **d-U(600)**, 20–25 min for **t-U(403)** and **t-U(5000)**, and >36 h for **d-U(4000)**. Following ageing and drying, the resultant **PDI-Sil**-ureasils were obtained as freestanding, transparent monoliths. However, tangible differences in the mechanical properties could be identified: the rigidity of the monoliths increased as the mass ratio of ICPTES to polyetheramine increased, such that **t-U(403)** is rigid

 This journal is © The Royal Society of Chemistry 2016

and difficult to bend or cut, while **d-U(600)** and **t-U(5000)** are reasonably flexible. Notably, **d-U(4000)** is elastomeric and highly resistant to contraction during drying.

Local structure of PDI-Sil-ureasils

Global structural characterisation of organic–inorganic hybrid materials is often challenging, due in part to the chemical dissimilarity of the constituents. Moreover, for low dopant concentrations, it can be difficult to spectroscopically resolve the specific contribution of the dopant molecule from the ureasil host matrix.[28,34] The PXRD patterns for all samples exhibit a primary band at 19.5–21.1°, with a shoulder at 12.2–13.5°, which is typical of these amorphous materials (Fig. S7, ESI†). The main peak at 21° is associated with the presence of ordering within the siliceous domains,[31] and from this, the structural unit distance, *d*, was determined to be 4.4 ± 0.2 Å (from Bragg's Law). The shoulder between 11.0° and 15.0° is attributed to in-plane ordering of other intra-siloxane domains[31] and shows significant resolution in the low MW ureasils **t-U(403)** and **d-U(600)**. The coherent length over which the structural unit survives was estimated to be 10.2 ± 0.7 Å (from the Scherrer equation). The PXRD patterns are predominantly influenced by the ureasil host and at the concentration studied here, the introduction of **PDI-Sil** does not appear to affect the global structure of the siliceous network.

The ^{29}Si MAS-NMR spectra of all **PDI-Sil**-ureasils contain three broad signals characteristic of T_1, T_2 and T_3 units (Fig. S8, ESI†). The T_2 signal ($(R'Si(OSi)_2)(OR)$) is the dominant environment, with the T_3 ($(R'Si(OSi)_3)$) and T_1 ($(R'Si(OSi)\text{-}(OR)_2)$) peaks providing a smaller contribution. The T_1 signal is completely absent from the **t-U(403)** samples, which also show a higher calculated degree of condensation, *C*, of ∼80%.[48] This high degree of condensation of the **t-U(403)** system is rational if the low MW and tri-branched structure of the corresponding Jeffamine precursor are considered. *C* ranges from 67–71% for the other systems (Table S1, ESI†), which is in reasonable agreement with other ureasil-type materials.[34,49] The absence of the T_0 signal (−44 ppm) indicates that there is no unreacted precursor remaining. ^{13}C CP/MAS-NMR measurements confirm that **PDI-Sil-t-U(403)** (and **t-U(403)**) behave as typical rigid solids and are in excellent agreement with those previously reported for tri-ureasils of this type (Fig. S9, ESI†).[45] In contrast, **PDI-Sil-t-U(5000)**, **PDI-Sil-d-U(4000)**, **PDI-Sil-d-U(600)**, and their undoped analogues, are highly mobile and do not yield appreciable signals under cross-polarisation. This is consistent with the high degree of elastomericity of the macroscopic samples. As expected, direct evidence of the **PDI-Sil** component cannot be observed due to its low concentration. However, some minor relative intensity differences are observed between the **PDI-Sil**-ureasils and their undoped counterparts, suggesting that the **PDI-Sil** must have some impact on the structure of the material (Fig. S9, ESI†).

Vibrational spectroscopy provides valuable insight into the influence of the preparation method and/or introduction of dopants on the local structure of ureasils.[50,51] In particular, the Amide I region of the FTIR spectrum (1600–1800 cm^{-1}) can provide diagnostic information about the specificity and extent of hydrogen bonding interactions associated with the urea linkages (Fig. 3). Gaussian deconvolution reveals that 3–5 components are required to model the Amide I band, which is typical of ureasils (see Table S3, ESI†).[50,52] The bands at *ca.* 1707 (Peak 1), 1660 (Peak 2) and 1635 (Peak 3) cm^{-1} are common to all samples, and are assigned to stretching vibrations associated with C═O groups located in disordered hydrogen-bonded polyoxyethylene (POE)/polyoxypropylene (POP)–urea associations of increasing strength (Peak 1 and 2), and C═O groups present in significantly more ordered hydrogen-bonded urea–urea aggregates (Peak 3).[52] With the exception of **t-U(5000)**, all samples also exhibit a minor peak (2–5%) at *ca.* 1745 cm^{-1} (Peak 4), attributed to non-hydrogen bonded urea groups.[52] For **d-U(4000)**, a component at *ca.* 1727 cm^{-1} is also present, ascribed to the same origin as Peaks 1–3. A higher HCl concentration was used to induce gelation of this sample, which has previously been shown to affect the proportion of POP/urea aggregates in tri-ureasils.[50]

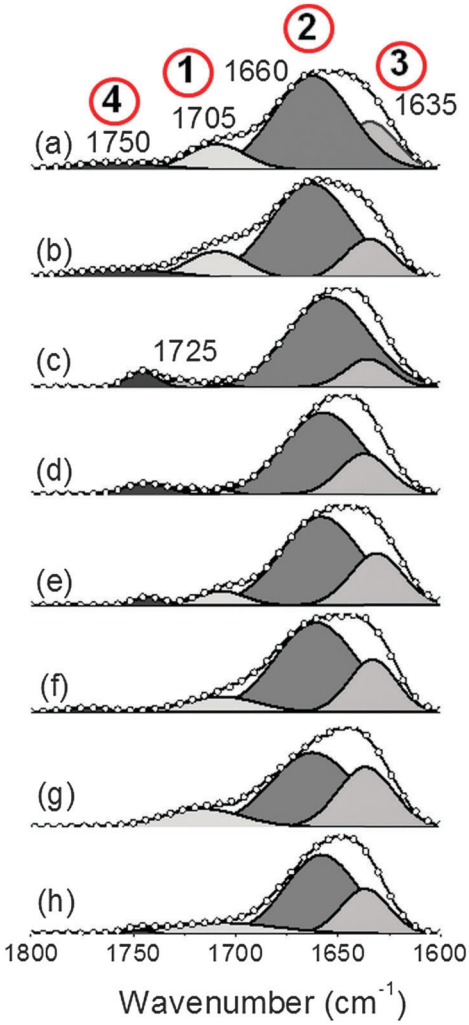

Fig. 3 Gaussian fits to the Amide I region of the FTIR spectrum of (a) **d-U(600)**, (b) **PDI-Sil-d-U(600)**, (c) **d-U(4000)**, (d) **PDI-Sil-d-U(4000)**, (e) **t-U(403)**, (f) **PDI-Sil-t-U(403)**, (g) **t-U(5000)**, (h) **PDI-Sil-t-U(5000)**. The circled numbers represent the peaks described in the text.

The incorporation of **PDI-Sil** does not affect the hydrogen-bonding interactions in the shorter chain ureasils. However, for **PDI-Sil-d-U(4000)**, an 8% increase in the contribution from ordered, hydrogen-bonded urea–urea aggregates (Peak 3) is observed, at the expense of weaker POP/urea interactions (Peaks 1 and 2). In contrast, for **PDI-Sil-t-U(5000)**, the opposite trend is revealed. Given that **PDI-Sil** is functionalised on both extremities with hydrolysable alkoxysilane moieties, it seems probable that it bridges individual UPTES chains. The spectral changes may infer that this arrangement facilitates better packing for the linear chain **PDI-Sil-d-U(4000)**, whereas it increases disorder in the tripodal **PDI-Sil-t-U(5000)**. For all samples, no increase in the contribution of Peak 4 is observed, indicating that incorporation of **PDI-Sil** does not lead to significant destruction of urea/urea or POE/POP/urea aggregates and that the formation of stacked dimers is improbable.

Stability studies

The thermal stability of **PDI-Sil**-ureasils is controlled by the ureasil host matrix. The obtained thermograms are in excellent agreement with those previously reported for di-[53] and tri-ureasils,[51] with the onset of sample decomposition observed at ~250–270 °C and ~280 °C, respectively (Fig. S10, ESI†). **PDI-Sil** itself exhibits an extremely high thermal stability (T_{onset} – 379 °C, Fig. S11, ESI†) but its incorporation within the ureasil does not influence the thermal properties significantly. However, the thermal stability of **PDI-Sil**-ureasils considerably surpasses the moderate operating temperatures of a solar cell in hot climatic conditions (~80–95 °C).[54] The photostability of **PDI-Sil-t-U(5000)** was investigated as a representative sample (Fig. S12, ESI†). Upon continuous irradiation at 370 nm over a 5 h period, no significant decrease in the integrated intensity of the **PDI-Sil** emission was observed, for either monolithic or thick film samples.

Steady-state photoluminescence studies

Under UV illumination (λ_{ex} = 365 nm), undoped di-ureasils/tri-ureasils exhibit blue photoluminescence, in agreement with previous reports for **d-U(600)** and **t-U(5000)** (see Fig. S13, ESI†).[44,51] This is characterised by a broad band in the photoluminescence (PL) spectrum centred between 350–500 nm, as illustrated in Fig. 4a for **t-U(403)**. The emission maximum is strongly dependent on the excitation energy, red-shifting to longer wavelengths as λ_{ex} increases (see Fig. S15–S17, ESI† for other undoped ureasils). A similar trend is observed in the corresponding excitation spectrum (Fig. S14, ESI† for **t-U(403)** and Fig. S15–S17, ESI† for other undoped ureasils). This excitation/emission energy dependence is typical of ureasil-type materials and has been previously ascribed to the convolution of electron–hole recombinations occurring at donor–acceptor pairs localised at the urea bridges and in the siliceous nanodomains.[44] The photoluminescence quantum yields (Φ_{PL}) of the undoped ureasils determined upon excitation at 350 nm are in good agreement with previously reported values for related di/tri-ureasils (Table 1).[31,50] The magnitude of Φ_{PL} follows the order **d-U(4000)** > **t-U(403)** > **t-U(5000)** > **d-U(600)**. An increase in the organic polymer chain length for linear di-ureasils has previously been shown to increase the Φ_{PL}.[55]

Ureasils have been shown to act as efficient energy donors while acting as hosts for emissive molecules/complexes.[34,55] Fig. 4b shows the PL spectra of **t-U(403)** and **d-U(600)** and the UV/Vis absorption and PL spectra of **PDI-Sil** in THF. Significant spectral overlap between the **t-U(403)**/**d-U(600)** emission and the **PDI-Sil** absorption is observed, indicating that efficient Förster resonance energy transfer (FRET) and/or radiative (trivial) energy transfer from the ureasil donor (D) to the **PDI-Sil** acceptor (A) may occur, depending on the D–A separation and the relative orientation of the absorption and emission transition dipole moments.

For all **PDI-Sil**-ureasils, at excitation wavelengths between 330–400 nm, the PL spectrum is dominated by the **PDI-Sil** emission, centred between 550–750 nm. However, distinct differences are observed between samples in the ureasil emission region (380–500 nm). For **PDI-Sil-t-U(403)** and **PDI-Sil-d-U(4000)** a broad emission band, whose relative intensity and peak maxima are modulated by the excitation energy is observed (Fig. 4c and Fig. S19, ESI†). In contrast, the ureasil provides only a minor contribution to the PL spectra of **PDI-Sil-t-U(5000)** and **PDI-Sil-d-U(600)** (Fig. 4d and Fig. S19, ESI†). Accordingly, the emission colour of samples under UV illumination is also different: **PDI-Sil-t-U(403)** and **PDI-Sil-d-U(4000)** are pink, while **PDI-Sil-t-U(5000)** and **PDI-Sil-d-U(600)** are orange. For λ_{ex} < 370 nm, direct excitation of **PDI-Sil** is expected to be negligible, thus suggesting that the observed emission is a result of energy transfer from the ureasil host. The corresponding excitation spectra reveal a small band in the ureasil excitation region upon detection in the **PDI-Sil** emission band, also inferring the occurrence of energy transfer (Fig. 4c and d).[56] The photoluminescence quantum yields of the **PDI-Sil**-ureasils upon excitation at 520 nm (selective excitation of **PDI-Sil**) are in the range of Φ_{PL} = 76–87% and follow the order **d-U(4000)** > **t-U(5000)** > **t-U(403)** > **d-U(600)** (see Table S4, ESI†).[57] We note that the incorporation of **PDI-Sil** into the ureasil does not result in a significant decrease in Φ_{PL} compared to the solution value (Φ_{PL} = 90% in THF). In a previous study, we observed that physical immobilisation (Class I hybrid) of the related perylene diimide Lumogen Red LR305 into **d-U(600)** at the same loading (0.005 wt%) resulted in a 20 nm shift in the emission maximum, band broadening and a decrease in Φ_{PL}.[33] However, none of these phenomena are observed for the **PDI-Sil**-ureasils, suggesting that covalent grafting leads to improved isolation of the lumophore compared with physical immobilisation.

Mechanism for ureasil to PDI-Sil energy transfer?

Both FRET and radiative (trivial) energy transfer require overlap between the emission spectrum of the donor and the absorption spectrum of the acceptor. Table 1 shows the calculated spectral overlap integrals (J_{DA}) for FRET obtained from:

$$J_{DA}(\lambda) = \int_0^\infty F_D(\lambda)\varepsilon_A(\lambda)\lambda^4 d\lambda \quad (1)$$

where F_D is the intensity of the D emission spectrum at wavelength λ to $\lambda + \Delta\lambda$, with the total intensity normalised to unity and ε_A is the molar absorption coefficient of A at wavelength λ. **d-U(600)** and **t-U(5000)** exhibit the largest J_{DA} values,

 This journal is © The Royal Society of Chemistry 2016

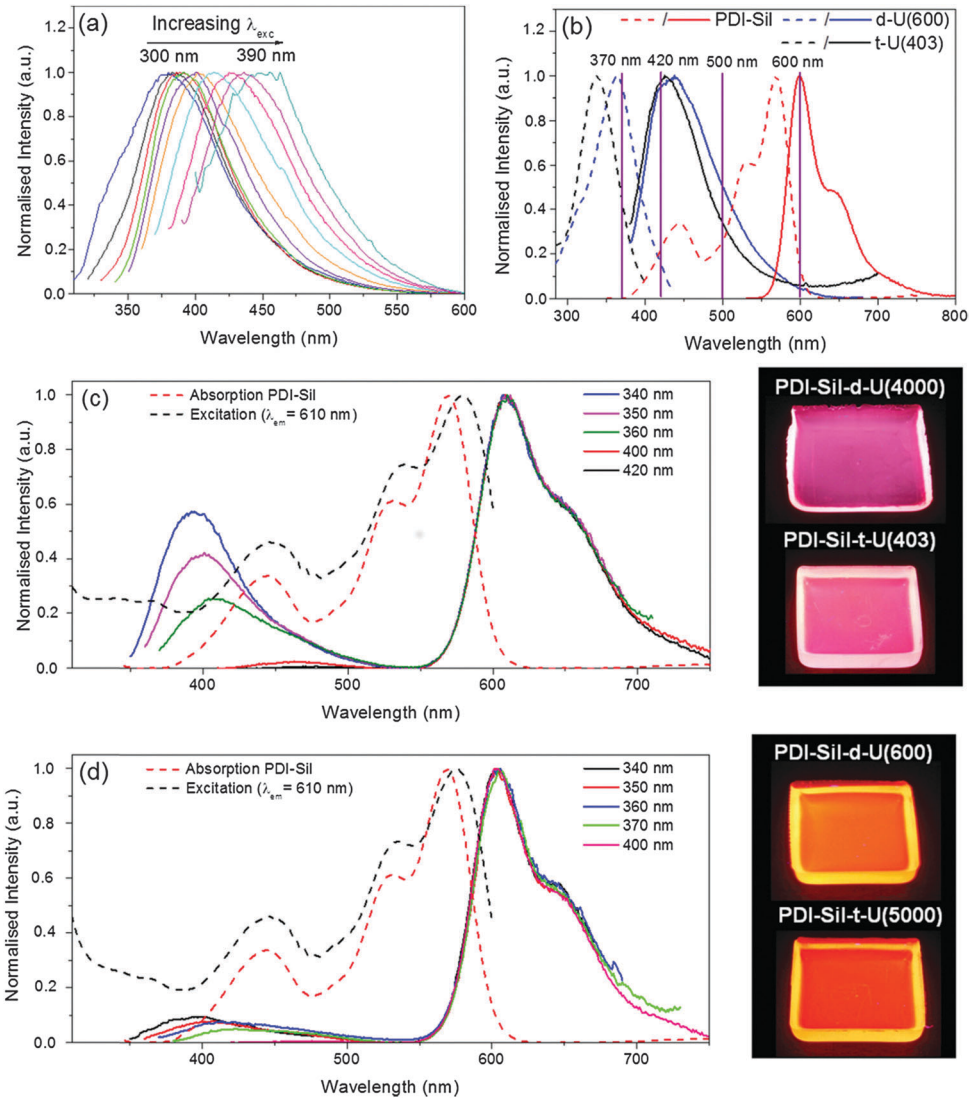

Fig. 4 Steady-state photoluminescence properties of undoped and **PDI-Sil**-ureasils. (a) PL emission of **t-U(403)** as a function of the excitation wavelength. (b) PL and excitation spectra for **t-U(403)** (black, λ_{ex} = 370 nm, λ_{em} = 420 nm), **d-U(600)** (blue, λ_{ex} = 365 nm, λ_{em} = 420 nm) and UV/Vis absorption and emission spectra for **PDI-Sil** (red, λ_{ex} = 590 nm in THF (1×10^{-6} mol dm^{-3})). The purple lines highlight the excitation (λ_{ex}) and emission (λ_{em}) wavelengths used in the ps-TCSPC experiments. Absorption spectrum of **PDI-Sil** in THF, PL emission spectra and excitation spectrum (λ_{em} = 610 nm) of (c) **PDI-Sil-t-U(403)** and (d) **PDI-Sil-t-U(5000)** and the corresponding photographs of **PDI-Sil**-ureasils under UV excitation (λ_{ex} = 365 nm). Emission spectra are shown as solid lines and excitation and UV/Vis absorption spectra are shown as dashed lines.

Table 1 Summary of the photophysical data obtained for undoped ureasils. J_{DA} and R_0 are the calculated spectral overlap integral and Förster distance for resonance energy transfer respectively, considering the ureasil as the donor (D) and **PDI-Sil** as the acceptor (A). Φ_{PL} is the photoluminescence quantum yield and $\langle\tau\rangle$ is the average lifetime for the emission decay detected at either 420 nm or 500 nm

Sample	J_{DA} (M^{-1} cm^3)	R_0 (nm)	Φ_{PL}[a] (%)	$\langle\tau\rangle$ (ns)
d-U(600)	4.73×10^{-14}	2.43	3.8 ± 0.2	4.61 (420 nm) 5.91 (500 nm)
d-U(4000)	4.36×10^{-14}	2.82	9.9 ± 0.3	6.35 (420 nm) 8.53 (500 nm)
t-U(403)	4.12×10^{-14}	2.75	9.1 ± 1.7	7.60 (420 nm) 8.97 (500 nm)
t-U(5000)	4.72×10^{-14}	2.73	7.5 ± 0.1	5.85 (420 nm) 7.35 (500 nm)

[a] Average of three independent measurements (λ_{ex} = 350 nm).

which infers that energy transfer should be most efficient in the corresponding **PDI-Sil**-ureasils. This is in good agreement with the PL spectra of **PDI-Sil-d-U(600)** and **PDI-Sil-t-U(5000)**, which show only a small contribution from the ureasil emission. The corresponding Förster distance, R_0, the distance at which the FRET efficiency is 50% efficient, was calculated from:

$$R_0^6 = \frac{9000(\ln 10)\kappa^2 \Phi_D J_{DA}}{128\pi^5 n^4 N_A} \quad (2)$$

where Φ_D is the photoluminescence quantum yield of the donor, n is the refractive index of the host ureasil (taken to be ~1.5) and N_A is Avogadro's number.[29] κ is the orientation factor, which describes the relative orientation of the transition dipoles of the donor and acceptor and was taken to be 2/3,

which assumes an isotropic orientation of the donor and acceptor.[58]

The calculated R_0 values, which take into account differences in Φ_{PL} for the energy donor and the J_{DA}, are essentially identical for all except **d-U(600)** (Table 1), which is somewhat surprising given the significant differences observed in the emission spectra of the **PDI-Sil**-ureasils. This result may indicate either that the observed energy transfer does not proceed solely *via* the FRET (non-radiative) mechanism or that the assumed orientation factor of 2/3 may not be applicable.

Picosecond time-correlated single photon counting (TCSPC) measurements were performed to further explore the energy transfer mechanism. From Fig. 4b, selective excitation of the ureasil and **PDI-Sil** is possible at λ_{ex} = 370 nm and λ_{ex} = 460 nm, respectively. Similarly, detection of the emission decay curves at λ_{em} = 420 nm and 500 nm enables isolation of the ureasil emission, while at λ_{em} = 600 nm the emission from **PDI-Sil** predominates. For the undoped ureasils, the decay curves at both detection wavelengths are best modelled with three discrete exponential components (τ_i) (see Fig. 5). The fitting data are summarised in Table S5, ESI† and are in excellent agreement with previous reports for **d-U(600)**, which displays three emission lifetimes: $\tau_1 < 1$ ns, $\tau_2 \approx 2.0$–3.5 ns and $\tau_3 \approx 9.0$–11.5 ns.[34,59] The average lifetimes, $\langle\tau\rangle$ (Table 1), follow the order **t-U(403)** > **d-U(4000)** > **t-U(5000)** > **d-U(600)** which is in good agreement with the trend observed for Φ_{PL}. At λ_{em} = 500 nm, $\langle\tau\rangle$ is longer for all samples, due to a decrease in the pre-exponential factor, α_i, corresponding to τ_1, accompanied by an increase in α_2, τ_2 and τ_3. Previously, time-resolved emission studies performed at 14 K showed the predominance of the higher-energy component from silica defects at 1–5 ms, with the emergence of the lower-energy component associated with the NH centres at longer times (>10 ms).[44] Given the spectral dominance of the siliceous centred emission at 420 nm and urea-centred emission at 500 nm, it is therefore reasonable to assign these contributions to τ_1 and τ_3, respectively. The concomitant decrease in α_1 and increase in α_2 suggest interconversion between the species is responsible for these decay pathways. We have recently shown that excitation energy transfer between the siliceous and urea domains occurs in **d-U(600)**,[34] and we attribute τ_2 to relaxation of these emissive centres following population by energy transfer.

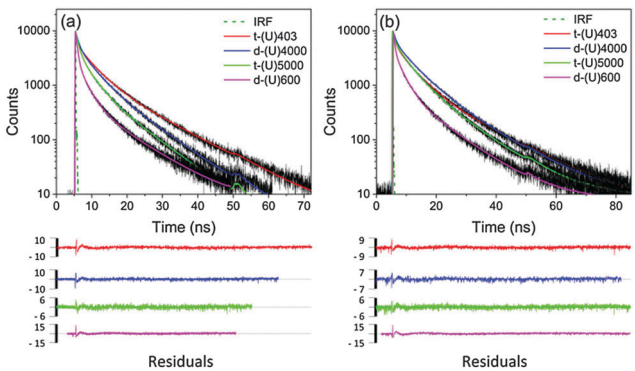

Fig. 5 Emission decay curves (solid black lines) and fits (coloured lines) for undoped ureasils upon excitation at 370 nm and detection at (a) 420 nm and (b) 500 nm. The weighted residuals for each fit and the instrument response function (IRF, dotted line) are also shown.

If the **PDI-Sil** emission is considered directly, it is challenging to spectroscopically isolate contributions from reabsorption and/or aggregation phenomena. Under steady-state conditions both processes lead to a decrease in Φ_{PL}, a red-shift in the emission maximum and/or a change in the spectral shape.[57,60,61] None of these spectral characteristics are evident in the photoluminescence spectra of the **PDI-Sil**-ureasils. Similarly, if present, both pathways should give rise to multiexponential emission decay kinetics.[62] For **PDI-Sil**-ureasils, excitation at 370 nm gives rise to a monoexponential decay curve (λ_{em} = 600 nm) with a characteristic lifetime of ~6.8–7.0 ns, which is in excellent agreement with the emission lifetime of **PDI-Sil** in THF (Fig. S22, ESI†). This may indicate that covalent-grafting of **PDI-Sil** to the ureasil prevents the formation of dimers or stacked aggregates, which has been demonstrated to result in multiexponential emission decay.[47] However, if reabsorption effects were significant in these materials, a change in the emission lifetime would be expected, which is also not the case.[62] We suggest that covalent grafting of **PDI-Sil** to the ureasil may potentially reduce the efficiency of energy transfer, either through better isolation of individual fluorophores within the matrix (thereby increasing the D–A distance) or by reducing the overlap of the absorption and emission transition dipole moments.

Detection of the emission in the ureasil region reveals a triexponential decay curve, whose lifetimes and pre-exponential factors are of a similar order of magnitude as the undoped analogues (see Table S6, ESI†). The **PDI-Sil**-ureasils are generally longer lived than the parent ureasils, and show the same trend for the variation in α_i and τ_i on changing λ_{em} from 420 nm to 500 nm. The observation of **PDI-Sil** emission upon excitation into the ureasil suggests that energy transfer occurs; however, this would be expected to be accompanied by a significant decrease in one or more of the ureasil lifetimes if it proceeds solely by the FRET mechanism, which is not the case. The results suggest that the energy transfer efficiency is affected by the packing and orientation of the **PDI-Sil** within the ureasil host. **PDI-Sil** shows better spectral overlap with the urea-centred emission (2.80–3.19 eV), but α_3 and τ_3 are effectively unchanged upon incorporation of the fluorophore into the ureasil (Table S6, ESI†).

This may be understood by considering that **PDI-Sil** is grafted to the siliceous framework and thus may be spatially isolated from urea-rich domains. However, a global decrease in α_1 and τ_1, which are ascribed to siliceous centred emission (2.99–3.41 eV), is also not observed upon incorporation of **PDI-Sil** into the ureasil. Conventionally, FRET is considered to occur in the short-range (nanoscale) D–A separation with an R^{-6} dependence associated with dipole–dipole coupling, whilst radiative transfer is assumed to operate for D–A pairs separated by distances greater than optical wavelengths and exhibits an R^{-2} dependence.[63] The absence of any significant changes in the ureasil lifetime(s) in the presence of the **PDI-Sil** acceptor suggests that energy transfer predominantly occurs *via* a radiative mechanism in these samples, which may be masking any short range dipole–dipole interactions.[64] However, a unified

 This journal is © The Royal Society of Chemistry 2016

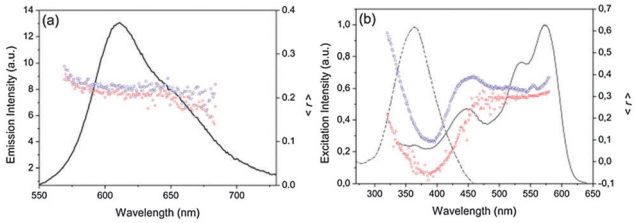

Fig. 6 Steady-state anisotropy of the fluorescence (a) emission (λ_{ex} = 500 nm) and (b) excitation (λ_{em} = 630 nm) of **PDI-Sil-d-U(600)** (red open squares) and **PDI-Sil-d-U(4000)** (blue open circles). The emission and excitation spectra (black lines) obtained using non-polarised light are shown for comparison.

theory based on quantum electrodynamics has been developed by Andrews and co-workers, which indicates that the FRET and radiative mechanisms are in fact the short- and long-range asymptotes of a single mechanism that necessarily requires coupling of the donor and acceptor transition dipole moments.[65] The observed difference in the energy transfer tendencies for different **PDI-Sil**-ureasils may therefore arise due to a combination of low spatial proximity and/or poor coupling of the D–A transition dipole moments. The differences in the global D–A distances may be understood by considering the MW and branching of the Jeffamine precursors: **t-U(403)** has the shortest branch length (~2 r.u. per chain), followed by **d-U(600)** (~13 r.u. per chain) and **t-U(5000)** (~28 r.u. per chain). Only **d-U(4000)** exhibits a distinctly different branch length (~68 r.u. per chain). This suggests that the chain length is the dominant factor in controlling the placement of the lumophore within the ureasil matrix, with **PDI-Sil-d-U(600)** and **PDI-Sil-d-U(4000)** exhibiting contrasting PL behaviour. The branching of the ureasil backbone apparently influences the PL properties to a lesser extent.

In an attempt to unravel the contribution of lumophore orientation on the energy transfer efficiency, preliminary steady-state fluorescence anisotropy measurements were performed on **PDI-Sil-d-U(600)** and **PDI-Sil-d-U(4000)**. As expected, the anisotropy, $\langle r \rangle$, remains constant across the **PDI-Sil** emission band (selective excitation of **PDI-Sil**), with an average value of ~0.2 for both samples (Fig. 6a). Similarly, in the corresponding excitation anisotropy spectrum, $\langle r \rangle$ remains effectively constant across the $S_0 \rightarrow S_1$ absorption band (500–620 nm), with a value of ~0.3 (Fig. 6b). However, between 380–460 nm, a significant dip in $\langle r \rangle$ to ~0.1 and ~−0.1 is revealed for **PDI-Sil-d-U(4000)** and **PDI-Sil-d-U(600)**, respectively. We note that anisotropy measurements are strongly influenced by scattering and reabsorption processes and that the measured values for these samples should not be interpreted as absolute. However, the significant decrease in $\langle r \rangle$ in the spectral region that overlaps with the ureasil emission, particularly for **PDI-Sil-d-U(600)**, suggests that energy transfer processes may be at play and may provide the first hint that an anisotropic orientation of donor and acceptor molecules exists.

Conclusions

We have shown that covalently grafting a perylene carboxdiimide to the siliceous framework within an ureasil host is an effective approach to isolate the fluorophore. This has the advantage of switching off several non-radiative deactivation pathways, which include the formation of stacked aggregates/dimers and re-absorption/re-emission processes. Ps-TCSPC lifetime measurements reveal monoexponential decay kinetics for the **PDI-Sil** emission, supporting the theory that the fluorophore molecules are well-dispersed in the ureasil and do not form molecular aggregates. The nature of the organic backbone of the ureasil was shown to result in dramatic differences in the energy transfer efficiency, which provides a means of probing the spatial distribution of the lumophore within the ureasil. This phenomenon warrants further investigation and linear dichroism and time-resolved fluorescence anisotropy measurements are planned to further investigate the orientation of the absorption and emission transition dipole moments.

Given that ureasils have already been demonstrated as waveguides, this insight should allow us to design highly efficient LSCs in which the fluorophore is directly integrated into the waveguide at a preferential orientation to minimise fluorophore-centred optical losses. Moreover, it has recently been shown significant anisotropic electrical conduction can be achieved through the long-range orientation of perylene bisimide-based organosilanes within a silica scaffold,[19] suggesting that this approach may also provide an interesting route to organic–inorganic hybrid devices exhibiting good electrical conductivities.

Acknowledgements

The authors thank Michèle Chevrier for assistance with the **PDI-Sil** synthesis and Claire Boulbet for help with preliminary photoluminescence experiments. Solid-state NMR spectra were obtained at the EPSRC UK National Solid-state NMR Service at Durham. This work was supported by the Science Foundation Ireland under Grant No. 12/IP/1608. NWF thanks the Irish Research Council for a Government of Ireland postgraduate studentship. The authors acknowledge financial support from the European Commission under the Seventh Framework Programme by means of the grant agreement for the Integrated Infrastructure Initiative No. 262348 European Soft Matter Infrastructure (ESMI). Support from COST action MP1202 (HINT – Hybrid Interfaces) and the Ireland-France "Hubert Curien Ulysses" programme (grant no. 31998ZF) are gratefully acknowledged.

Notes and references

1 A. Mishra and P. Bäuerle, *Angew. Chem., Int. Ed.*, 2012, **51**, 2020.
2 J. Roncali, *Acc. Chem. Res.*, 2009, **42**, 1719.
3 X. Guo, M. Baumgarten and K. Müllen, *Prog. Polym. Sci.*, 2013, **38**, 1832.
4 C. Wu and D. T. Chiu, *Angew. Chem., Int. Ed.*, 2013, **52**, 3086.
5 Y. He, W. Hong and Y. Li, *J. Mater. Chem. C*, 2014, **2**, 8651.
6 S. Rochat and T. M. Swager, *Angew. Chem., Int. Ed.*, 2014, **53**, 9792.
7 Z. B. Henson, K. Müllen and G. C. Bazan, *Nat. Chem.*, 2012, **4**, 699.

8 R. C. Evans, *J. Mater. Chem. C*, 2013, **1**, 4190.
9 T. Förster and K. Kasper, *Z. Phys. Chem.*, 1954, **1**, 275.
10 A. C. Grimsdale, K. L. Chan, R. E. Martin, P. G. Jokisz and A. B. Holmes, *Chem. Rev.*, 2009, **109**, 897.
11 E. Aharon, A. Albo, M. Kalina and G. L. Frey, *Adv. Funct. Mater.*, 2006, **16**, 980.
12 K. V. Rao, A. Jain and S. J. George, *J. Mater. Chem. C*, 2014, **2**, 3055.
13 P. C. Marr, K. McBride and R. C. Evans, *Chem. Commun.*, 2013, **49**, 6155.
14 G. Kickelbick, *Hybrid Materials: Synthesis, Characterization, and Applications*, Wiley-VCH, Weinheim, 2006.
15 R. C. Evans, A. G. Macedo, S. Pradhan, U. Scherf, L. D. Carlos and H. D. Burrows, *Adv. Mater.*, 2010, **22**, 3032.
16 S. Clément, A. Tizit, S. Desbief, A. Mehdi, J. De Winter, P. Gerbaux, R. Lazzaroni and B. Boury, *J. Mater. Chem.*, 2011, **21**, 2733.
17 R. C. Evans and P. C. Marr, *Chem. Commun.*, 2012, **48**, 3742.
18 D. Yan, J. Lu, M. Wei, D. G. Evans and X. Duan, *J. Phys. Chem. B*, 2009, **113**, 1381.
19 N. Mizoshita, T. Tani and S. Inagaki, *Adv. Funct. Mater.*, 2011, **21**, 3291.
20 S. Neyshtadt, J. P. Jahnke, R. J. Messinger, A. Rawal, T. Segal Peretz, D. Huppert, B. F. Chmelka and G. L. Frey, *J. Am. Chem. Soc.*, 2011, **133**, 10119.
21 M. Schneider and K. Müllen, *Chem. Mater.*, 2000, **12**, 352.
22 M. Kubo, C. Takimoto, Y. Minami, T. Uno, T. Itoh and M. Shoyama, *Macromolecules*, 2005, **38**, 7314.
23 D. Chandra, T. Yokoi, T. Tatsumi and A. Bhaumik, *Chem. Mater.*, 2007, **19**, 5347.
24 D. Chandra, S. K. Das and A. Bhaumik, *Microporous Mesoporous Mater.*, 2010, **128**, 34.
25 J. M. Behrendt, A. B. Foster, M. C. McCairn, H. Willcock, R. K. O'Reilly and M. L. Turner, *J. Mater. Chem. C*, 2013, **1**, 3297.
26 S. C. Nunes, V. de Zea Bermudez, M. M. Silva, M. J. Smith, D. Ostrovskii, R. A. S. Ferreira, L. D. Carlos, J. Rocha, A. Gonçalves and E. Fortunato, *J. Mater. Chem.*, 2007, **17**, 4239.
27 L. D. Carlos, R. A. S. Ferreira, V. de Zea Bermudez and S. J. L. Ribeiro, *Adv. Funct. Mater.*, 2001, **11**, 111.
28 N. Willis-Fox, M. Kraft, J. Arlt, U. Scherf and R. C. Evans, *Adv. Funct. Mater.*, 2016, **26**, 532.
29 D. C. Oliveira, A. G. Macedo, N. J. O. Silva, C. Molina, R. A. S. Ferreira, P. S. André, K. Dahmouche, V. de Zea Bermudez, Y. Messaddeq, S. J. L. Ribeiro and L. D. Carlos, *Chem. Mater.*, 2008, **20**, 3696.
30 C. M. S. Vicente, P. P. Lima, V. de Zea Bermudez, L. D. Carlos, P. S. André and R. A. S. Ferreira, *Opt. Express*, 2014, **22**, 27159.
31 M. C. Gonçalves, V. de Zea Bermudez, R. A. S. Ferreira, L. D. Carlos, D. Ostrovskii and J. Rocha, *Chem. Mater.*, 2004, **16**, 2530.
32 M. M. Nolasco, P. M. Vaz, V. T. Freitas, P. P. Lima, P. S. André, R. A. S. Ferreira, P. D. Vaz, P. Ribeiro-Claro and L. D. Carlos, *J. Mater. Chem. A*, 2013, **1**, 7339.
33 A. Kaniyoor, B. McKenna, S. Comby and R. C. Evans, *Adv. Opt. Mater.*, 2016, **4**, 444.
34 N. Willis-Fox, A.-T. Marques, J. Arlt, U. Scherf, L. D. Carlos, H. D. Burrows and R. C. Evans, *Chem. Sci.*, 2015, **6**, 7227.
35 G. Seybold and G. Wagenblast, *Dyes Pigm.*, 1989, **11**, 303.
36 M. G. Debije and P. P. C. Verbunt, *Adv. Energy Mater.*, 2012, **2**, 1.
37 J. L. Banal, K. P. Ghiggino and W. W. H. Wong, *Phys. Chem. Chem. Phys.*, 2014, **16**, 25358.
38 G. D. Gutierrez, I. Coropceanu, M. G. Bawendi and T. M. Swager, *Adv. Mater.*, 2016, **28**, 497.
39 Huntsman International LLC, Products, http://www.huntsman.com/performance_products/a/Products, accessed September 2015.
40 E. Gratton and J. Beechem, *Global WE (software)*, Laboratory for Fluorescence Dynamics, University of California, Irvine, CA, 2004.
41 D. Dotcheva, M. Klapper and K. Müllen, *Macromol. Chem. Phys.*, 1994, **195**, 1905.
42 T. Zhang, D. Sun, X. Ren, L. Liu, G. Wen, Z. Ren, H. Li and S. Yan, *Soft Matter*, 2013, **9**, 10739.
43 T. Zhang, Z. Ren, X. Sun and S. Yan, *Phys. Chem. Chem. Phys.*, 2015, **17**, 23069.
44 L. D. Carlos, V. de Zea Bermudez, R. A. S. Ferreira, L. Marques and M. Assunção, *Chem. Mater.*, 1999, **11**, 581.
45 E. F. Molina, L. Marçal, H. W. Pereira de Carvalho, E. J. Nassar and K. J. Ciuffi, *Polym. Chem.*, 2013, **4**, 1575.
46 B. Fouzia, J. Ferguson, K. McKenna, L. E. McNamara, N. I. Hammer and H. Rathnayake, *New J. Chem.*, 2015, **39**, 2004.
47 F. Ito, H. Sato, Y. Ugachi, N. Oka, S. Ito and H. Miyasaka, *Photochem. Photobiol. Sci.*, 2015, **14**, 1896.
48 The degree of condensation of the siliceous network was determined from C (%) = 1/3(%T_1 + 2%T_2 + 3%T_3), using Gaussian deconvolution of the peaks to determine the relative population of each organosiloxane species.
49 P. P. Lima, R. A. S. Ferreira, S. A. Júnior, O. L. Malta and L. D. Carlos, *J. Photochem. Photobiol., A*, 2009, **201**, 214.
50 V. T. Freitas, P. P. Lima, V. de Zea Bermudez, R. A. S. Ferreira and L. D. Carlos, *Eur. J. Inorg. Chem.*, 2012, 5390.
51 V. T. Freitas, P. P. Lima, R. A. S. Ferreira, E. Pecoraro, M. Fernandes, V. de Zea Bermudez and L. D. Carlos, *J. Sol–Gel Sci. Technol.*, 2013, **65**, 83.
52 V. de Zea Bermudez, L. D. Carlos and L. Alcácer, *Chem. Mater.*, 1999, **11**, 569.
53 M. M. Silva, V. de Zea Bermudez, L. D. Carlos, A. Paula Passos de Almeida and M. J. Smith, *J. Mater. Chem.*, 1999, **9**, 1735.
54 N. Grossiord, J. M. Kroon, R. Andriessen and P. W. M. Blom, *Org. Electron.*, 2012, **13**, 432.
55 L. D. Carlos, R. A. S. Ferreira, R. N. Pereira, M. Assunção and V. de Zea Bermudez, *J. Phys. Chem. B*, 2004, **108**, 14924.
56 We note that the corresponding absorption are in excellent agreement with the observed excitation spectra, as shown in Fig. S20 (ESI†).
57 We note that for optically-thick samples, waveguiding of the emitted light and subsequent reabsorption of the emitted

 This journal is © The Royal Society of Chemistry 2016

photons may cause the measured Φ_{PL} to deviate from its true value. However, correction of Φ_{PL} to account for re-absorption/re-emission processes in these samples using the method described by Ahn *et al.* results in a negligible change in Φ_{PL} (81–88%) within experimental error for the PDI-Sil-ureasil samples reported here. See: T.-S. Ahn, R. O. Al-Kaysi, A. M. Müller, K. M. Wentz and C. J. Bardeen, *Rev. Sci. Instrum.*, 2007, **78**, 086105.

58 H. Y. Byun, I. J. Chung, H.-K. Shim and C. Y. Kim, *Macromolecules*, 2004, **37**, 6945.

59 L. Fu, R. A. S. Ferreira, M. Fernandes, S. C. Nunes, V. de Zea Bermudez, G. Hungerford, J. Rocha and L. D. Carlos, *Opt. Mater.*, 2008, **30**, 1058.

60 J. R. Lakowicz, *Principles of Fluorescence Spectroscopy*, Springer, New York, 2007, p. 57.

61 A. P. Green, K. T. Butler and A. R. Buckley, *Appl. Phys. Lett.*, 2013, **102**, 133501.

62 (*a*) R. O. Al-Kaysi, T. S. Ahn, A. M. Müller and C. J. Bardeen, *Phys. Chem. Chem. Phys.*, 2006, **8**, 3453; (*b*) R. Katoh, S. Sinha, S. Murata and M. Tachiya, *J. Photochem. Photobiol., A*, 2001, **145**, 23.

63 D. L. Andrews and G. Juzeliūnas, *J. Chem. Phys.*, 1991, **95**, 5513.

64 We note that identical PL spectra were obtained for the corresponding thick films of these samples. See Fig. S21, ESI†.

65 D. L. Andrews, *Chem. Phys.*, 1989, **135**, 195.